http://dx.doi.org/10.21577/0103-5053.20190085

J. Braz. Chem. Soc., Vol. 30, No. 9, 1789-1800, 2019
Printed in Brazil - ©2019 Sociedade Brasileira de Química

Article

Three Different Types of Activated Carbon and Manganese-Modified Activated Carbons as Deoxidizers for the Low-Concentration Coalbed Methane Deoxidation

Guojie Zhang, *,[a,b] *Peng Hou,*[a] *Yinghui Sun,*[a] *Ying Xu,*[a] *Haizhu Cheng*[a] *and Yongfa Zhang*[a]

[a]*Key Laboratory of Coal Science and Technology, Ministry of Education and Shanxi Province, Taiyuan University of Technology, 030024 Taiyuan, Shanxi, P. R. China*

[b]*College of Chemical Engineering, Qingdao University of Science and Technology, 53 Zhengzhou Road, 266042 Qingdao, P. R. China*

Different activated carbons and manganese-modified activated carbons were prepared as deoxidizers for the low-concentration coalbed methane deoxidation. The results show that the deoxidation performance of the different activated carbons is affected by raw materials for preparation of deoxidizers. One type of activated carbon exhibited the best performance of oxygen removal, due to the relatively low ash content and better adsorption performance. Experimental results show that the manganese-modified deoxidizers exhibit an excellent deoxidation efficiency at low temperature. At 200 °C, one kind of manganese-modified activated carbons decreased the oxygen content to less than 1 vol%, which could maintain about 600 min. This indicated that the addition of manganese greatly improved the reactivity of oxygen with activated carbon. Characterization results demonstrated that the physical structure and species types of oxygen of activated carbons, and manganese have important effects on the activity of deoxidizers in different temperature ranges.

Keywords: coalbed methane, activated carbon, deoxidizer, potassium permanganate

Introduction

Coalbed methane is a by-product of coal mining. It is a new type of clean energy. Coalbed methane extraction is mainly divided into two methods: ground and underground extraction. The coalbed methane extracted through the ground has high methane content and high utilization value. For coalbed methane extracted underground, the methane content is low and mixed with a large amount of air, resulting in an increased risk of explosion. This limits its utilization and pressure pipeline transportation, which is also the main factor that has been disrupting the large-scale utilization of coalbed methane. At present, coalbed methane with a CH_4 concentration lower than 30% is mainly treated by incineration destruction or dispersal, resulting in an annual discharge of up to 19 billion cubic meters, equivalent to more than 200 million tons of standard coal. This not only caused a lot of waste of resources, but also caused great damage to the ecological environment.[1,2] The development and utilization of low-concentration coalbed methane can not only improve the utilization rate of coalbed methane, make up for energy shortage, reduce greenhouse effect, develop low-carbon economy, reduce environmental pollution, but also reduce or avoid gas explosion accidents, which have a safety effect.[1] Therefore, the development and utilization of coalbed methane has attracted great attention from the state and society.

If the low concentration oxygen-containing coalbed methane is directly enriched and concentrated, the O_2 concentration would increase with the increase of CH_4 concentration. In the end, the concentration of O_2 reaches the explosive limit and increases the danger of operation. Therefore, deoxidation is a key constraint for the rational use of low-concentration oxygen-containing coalbed methane. There are lots of technical problems for coalbed methane deoxidation in home and abroad. At present, the main deoxidation technologies are as follows: low temperature cryogenic liquefaction separation,[3-6] membrane separation, pressure swing adsorption separation,[7-14] coke combustion deoxidation and catalytic combustion deoxidation.[15,16] However, there are some operational inconvenience and hidden dangers for low temperature separation method,

*e-mail: zhangguojie@tyut.edu.cn, zhgjdoc@126.com

membrane separation and pressure swing adsorption method. The carbon combustion deoxidation is through direct combustion reaction of coke with O_2 in coalbed methane to generate CO_2 and CO to remove O_2 from coalbed methane. Due to the higher reaction temperature, some CH_4 will be cleaved to form H_2. Thus, the most critical problem that we faced to solve is to reduce the reaction temperature and prevent the loss caused by CH_4 cracking.[17]

Previous studies[15,16] have found that using biomass charcoal as a deoxidizer, the deoxidation temperature can be reduced to less than 450 °C, and it also has a high deoxidation efficiency. In order to further reduce the deoxidation temperature and improve deoxidation efficiency, in this paper, three different kinds of activated carbon and manganese modified activated carbon were used as deoxidizer for the low-concentration coalbed methane deoxidation. The deoxidation efficiency and performance for different deoxidizer were investigated.

Experimental

Materials and sample preparation

Three different types of activated carbon (AC_x, x = 1, 2, 3) were obtained from market. AC_1 and AC_2 were prepared from different types of coal (AC_1 from Jiaozuo Activated Carbon Company, Henan, China; AC_2 form Xinhua Activated Carbon Company, Shanxi, China); AC_3 was prepared from coconut husk (from Hunan Activated Carbon Company, Hunan, China). The three activated carbon particles have a particle size of about 40-60 mesh. Analytical pure potassium permanganate was obtained from Aladdin Industrial Corporation (Shanghai, China). The activated carbon was washed with deionized water 5 times before use, then it was dried at 105 °C in a vacuum drying oven for 2 h. The modified activated carbon was prepared by wet impregnation using the appropriate potassium permanganate solutions. The mixtures were stirred at 25 °C for 4 h, and then filtered and calcined at 500 °C for 2 h, marked as Mn/AC_1, Mn/AC_2 and Mn/AC_3.

Deoxidation of coalbed methane (CBM)

Deoxidation of coalbed gas was carried out by a fixed-bed reactor. Prior to deoxidation reaction, 10 g of sample was dried under N_2 flow (100 mL min^{-1}) at 300 °C for 2 h. Then, the gas mixture containing 15% CH_4-15% O_2-70% N_2 with the total flow rate of 100 mL min^{-1} was introduced. The deoxidation performance was studied at different temperatures ranging from 200 to 350 °C. The gas composition and content were measured by a gas chromatograph (GC-950, Shanghai Haixin) with thermal conductivity detector (TCD) using 5A molecular sieves column. After the completion of the deoxidation, the reactor was cooled to 25 °C under a nitrogen atmosphere, and then a spent deoxidizer was taken out for characterization.

Characterization

The air was used as a carrier gas, and the weight change of the deoxidizer was evaluated by using a thermogravimetric (TG) analyzer (Netzsch STA 2500) at a heating rate of 10 °C min^{-1}. The analysis of surface chemistry was conducted using an X-ray photoelectron spectrometer (XPS) utilizing monochromatic Al Kα source (ESCALAB 250Xi, Thermo Scientific). The X-ray diffraction (XRD) analysis of samples was measured on a Bruker D8 Advance diffractometer.[8,9] Texture parameters of different deoxidizers were measured adopting a Builder Beishide 3H-2000PS2 automatic adsorption apparatus.[9] The Fourier transform infrared (FTIR) analyses of samples were recorded on Nicolet Galaxy 5020 FTIR spectrometer. The morphologies of deoxidizers were measured by scanning electron microscopy (SEM, Hitachi S-4800). The dispersion details of deoxidizers were carried out by an energy dispersive X-ray spectrometer (EDS, Quantax400). H_2-TPR (temperature-programmed reduction) was measured on Micromeritics AutoChem 2920 instrument.

Results and Discussion

Physical characterization of samples

Table 1 shows the surface area, average pore diameter and pore volume of the different activated carbon deoxidizers before and after reaction. BET (Brunauer-Emmett-Teller) and pore volume of activated carbon deoxidizers are relatively large before activation ($AC_{x\text{-}b}$, x = 1, 2, 3); after deoxidation ($AC_{x\text{-}a}$, x = 1, 2, 3), the values of all the activated carbon deoxidizers are greatly reduced. As shown in Table 1, the specific surface area for the $AC_{1\text{-}b}$ and $AC_{3\text{-}b}$ were similar before the reaction, 839.69 and 799.83 $m^2 g^{-1}$, respectively. The specific surface area for the $AC_{2\text{-}b}$ was larger: 930.72 $m^2 g^{-1}$. However, after deoxidation reaction, the value of AC_3 decreased the most, from 799.83 to 266.07 $m^2 g^{-1}$. The specific surface area has decreased by varying degrees after reaction; this could be attributed to how the materials were prepared, where AC_1 and AC_2 were prepared from different types of coal, and AC_3 was prepared from coconut husk. Due to the higher carbon content and lower ash content, AC_3 is favorable for the oxidative deoxidation. After

adding Mn modification, the specific surface area of all three different activated carbon deoxidizers are greatly decreased. The value of Mn/AC_2 decreased the most, from 492.78 to 39.99 $m^2 g^{-1}$. This indicates that the structure of AC_2 undergoes some obvious change after modification by potassium permanganate, and more active metal particles are adsorbed on the surface and pores.[18-20] This is conducive to the improvement of deoxidation activity. After deoxidation, the average pore diameter and pore volume of all activated carbon deoxidizers are greatly improved. Compared with the unmodified activated carbon AC_x (x = 1, 2, 3), the specific surface area, pore volume and pore size of modified deoxidizers obviously change after reaction, which indicates that the activated carbon modified by high potassium acid is more susceptible to oxidation with oxygen, causing slight collapse of surface and pores, and micropores disappear partially. It also shows that the activity of the deoxidizer increased after loading the active metal manganese, which is consistent with the experimental results.

Table 1. Structural property of the different activated carbon (AC) deoxidizers

Sample	BET surface area / ($m^2 g^{-1}$)	Average pore diameter / nm	Pore volume / ($cm^3 g^{-1}$)
AC_{1-b}	839.69	2.27	0.48
AC_{1-a}	801.32	2.28	0.46
AC_{2-b}	930.72	2.79	0.65
AC_{2-a}	927.01	2.81	0.65
AC_{3-b}	799.83	2.33	0.46
AC_{3-a}	266.07	2.48	0.17
Mn/AC_{1-b}	512.69	2.26	0.29
Mn/AC_{1-a}	163.01	3.60	0.15
Mn/AC_{2-b}	492.78	2.75	0.34
Mn/AC_{2-a}	39.99	7.20	0.07
Mn/AC_{3-b}	464.96	2.35	0.27
Mn/AC_{3-a}	106.51	4.21	0.11

Subscripted a and b represent the sample after and before the reaction, respectively. BET: Brunauer-Emmett-Teller.

Potassium permanganate modified activated carbon improved the deoxidation performance. Especially, Mn/AC_2 catalyst exhibited the best deoxidation performance at 200 °C. To explore the effects of physical parameters on the deoxidation performance of activated carbon deoxidizers, some samples were chosen to study N_2 physical adsorption/desorption performance. The results show that N_2 adsorption-desorption isotherms of the different deoxidizers samples were consistent with the presence of micropores and mesopores as each produced type-I and IV isotherms, suggesting that the AC_x structure was not altered by impregnation of Mn. The pore size distribution map before and after the reaction of different deoxidizer samples is also consistent with the BET analysis results.

In addition, by comparing the results of deoxidation test and characterization analysis, it can be seen that the surface area, pore size and pore volume of the deoxidizer are not the decisive factors for increasing the deoxidation activity. This is consistent with previous related researches[21,22] that the performance of activated carbon is more dependent on surface chemistry than physical properties.

H_2-TPR analysis

To investigate the effects of the potassium permanganate modification on the activated carbon deoxidizer reducibility, H_2-TPR experiment was carried out. Figure 1 presents the H_2-TPR profiles of Mn/AC_x (x = 1, 2, 3) deoxidizers with different activated carbon. The H_2-TPR profiles of three different kinds of deoxidizers displayed two reduction peaks, which are assigned to the stepwise reduction of manganese species. The higher temperature peak is ascribed to the reduction of Mn_2O_3/Mn_3O_4. The low temperature peak is attributed to the reduction of MnO_2/Mn_2O_3. Moreover, with activated carbon types from AC_1 to AC_3, there is a gradual shift of this low temperature reduction signal from 420 to 475 °C, confirming the formation of larger-sized bulk Mn_2O_3/Mn_3O_4 particles. The broad reduction peak on Mn/AC_2 and Mn/AC_3 deoxidizers indicates variations in the extent of manganese activated carbon interactions. Reduction peak temperature indicates the reducibility of deoxidizers, and the lower temperature of the reduction peak means stronger reducibility.[23-26] So the activity of

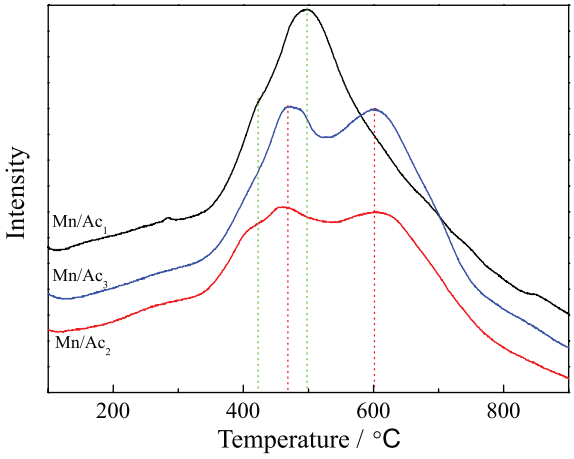

Figure 1. H_2-TPR profiles of Mn/AC_x (x = 1, 2, 3) deoxidizers before reaction.

Mn/AC_2 deoxidizers was higher than that of Mn/AC_1 and Mn/AC_3 deoxidizers at 200 °C.

X-ray diffraction analysis

In order to investigate the effect of deoxidizer phase composition and crystal structure on deoxidation performance, the prepared AC_x and Mn/AC_x deoxidizer were detected by the powder XRD patterns, as shown in Figure 2. For the AC_x deoxidizer (Figures 2a and 2b), a broadband in the range of 20-30° and a narrow peak at 2θ = 26° were detected due to the amorphous carbon structure, which corresponds to the (111) and (002) planes, respectively. In addition, it can be seen from the Figures 2a and 2b that a significant SiO_2 diffraction peak also appeared at 2θ = 20.8, 36.5, 50.1 and 68.1°, corresponding to (100), (110), (112) and (203) planes, respectively. It is suggested that SiO_2 is an important component of the AC_x deoxidizer.[27] By comparing the XRD crystal structure of AC_x before and after reaction, it can be found that the structure morphology of AC_1 and AC_2 deoxidizers hardly changed before and after reaction, while the carbon peak of AC_3 at 26.5 °C after deoxidation was significantly reduced. This indicates that the structural properties of AC_1 and AC_2 are relatively stable, and it is difficult to deoxidize at low temperatures, while AC_3 deoxidizer has higher activity, and at a lower temperature, it can undergo a deoxidation reaction. This is consistent with the experimental results.

After AC_x modification with potassium permanganate (Figure 2c), SiO_2, MnO and $MnCO_3$ diffraction peaks of Mn/AC_x deoxidizer were detected. SiO_2 diffraction peak appeared at 2θ = 30.6°, indexed to (110) reflection. The intensity of SiO_2 diffraction peak decreased because MnO and $MnCO_3$ on the AC_x surface covered a part of SiO_2. MnO diffraction peak appeared at 2θ = 34.9, 40.5, 58.7, 70.1 and 73.8°, corresponding to (111), (200), (220), (311) and (222) planes, respectively. $MnCO_3$ diffraction peak appeared at 2θ = 31.5°, indexed to (104) reflection. The MnO phase is generally considered to have excellent low temperature activity. MnO diffraction peak intensity at 2θ = 34.9 and 40.5° for Mn/AC_2 catalyst had a slight increase and the peak width was slightly narrow compared with Mn/AC_1

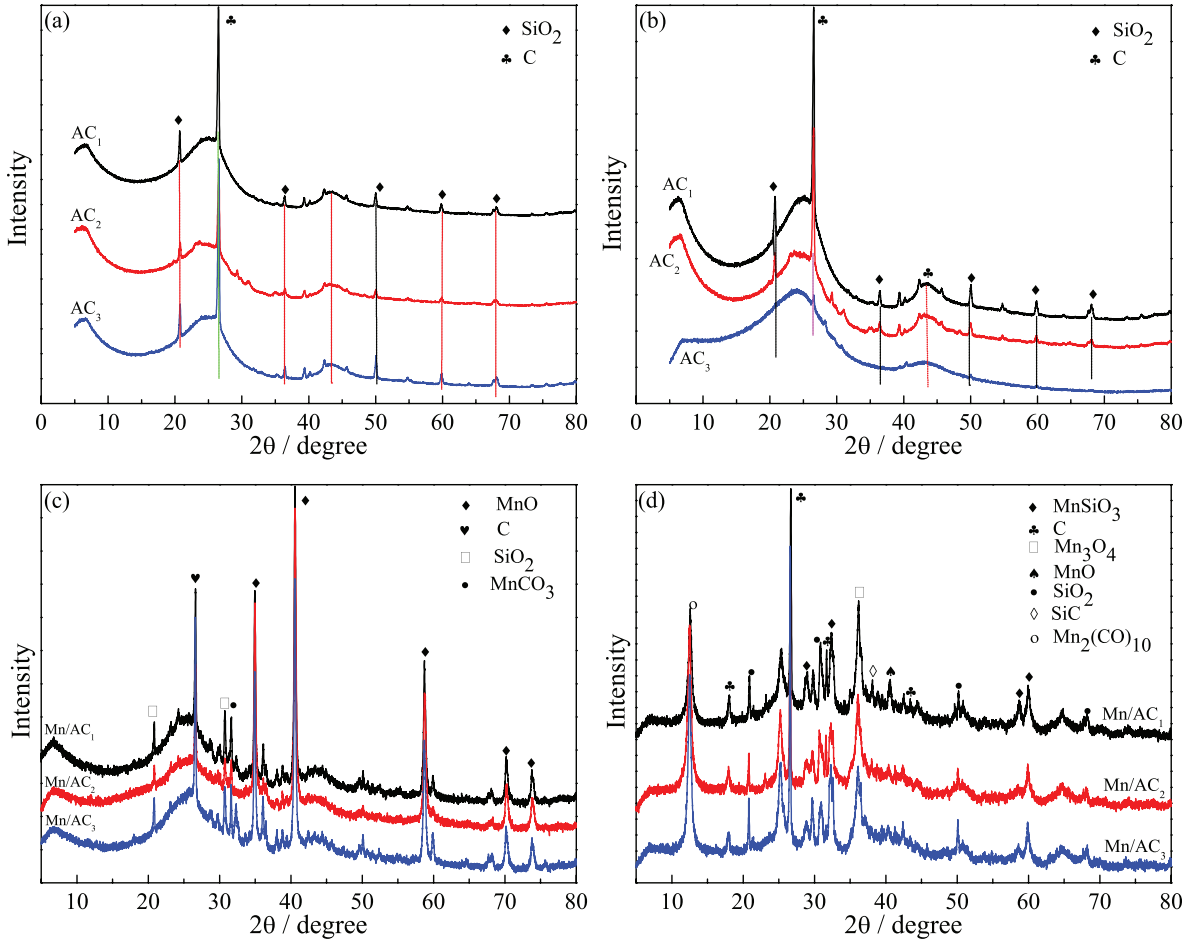

Figure 2. XRD patterns of before and after reaction of six deoxidizers: (a) AC_x (x = 1, 2, 3) before reaction; (b) AC_x (x = 1, 2, 3) after reaction; (c) Mn/AC_x (x = 1, 2, 3) before reaction; (d) Mn/AC_x (x = 1, 2, 3) after reaction.

and Mn/AC_3 deoxidizers, indicating the distribution uniformity of manganese active component on the AC_1 and AC_1 surface became poor, so the deoxidation rate of Mn/AC_1 and Mn/AC_3 deoxidizer were lower than those of Mn/AC_2 deoxidizer. However, no peak of MnO_2 was detected by XRD, indicating that it exists in the amorphous phase or is highly dispersed on the AC_x surface. The powder XRD patterns of calcined Mn/AC_x deoxidizer samples after reaction showed diffraction lines at $2\theta = 28.8, 32.2, 58.3$ and $59.7°$ typical for cubic $MnSiO_3$, and the diffraction signal at $2\theta = 36°$ is ascribed to Mn_3O_4 (Figure 2d). The intensity of MnO diffraction peaks became weak, suggesting that the MnO phase structure transforms to the Mn_3O_4 and $MnSiO_3$ phase. The activity of MnO was superior to that of Mn_3O_4 and $MnSiO_3$ at the low temperature. The formation of Mn_3O_4 and $MnSiO_3$ phase on the deoxidizer surface was to some extent responsible for the deoxidizer deactivation, so the deoxidation performance of Mn/AC_x decreased with the increase of the reaction time.

SEM and EDS analysis

Figure 3 shows the SEM images of the Mn/AC_1 and Mn/AC_2 deoxidizers before and after deoxidation reaction. It can be seen that the mapping of the two types of deoxidizers is completely different: the SEM images of Mn/AC_2 (Figure 3a) sample displayed the presence of MnO species (white spots) on the outer surface. Furthermore, for SEM images of Mn/AC_1, the MnO particles were agglomerated as clusters (Figure 3c), which appeared as white patches in SEM. Further, for Mn/AC_1 deoxidizer before and after deoxidation reaction, the surface morphologies have undergone significant changes as shown in Figure 3. After the deoxidation reaction, the surface of the sample became loose, mainly due to the participation of some carbon materials. Therefore, the surface of the sample is covered with a layer of gray matter, and at the same time, some pores in the deoxidizer are collapsed due to the reaction.[20,28-30] It is consistent with the result of BET analysis.

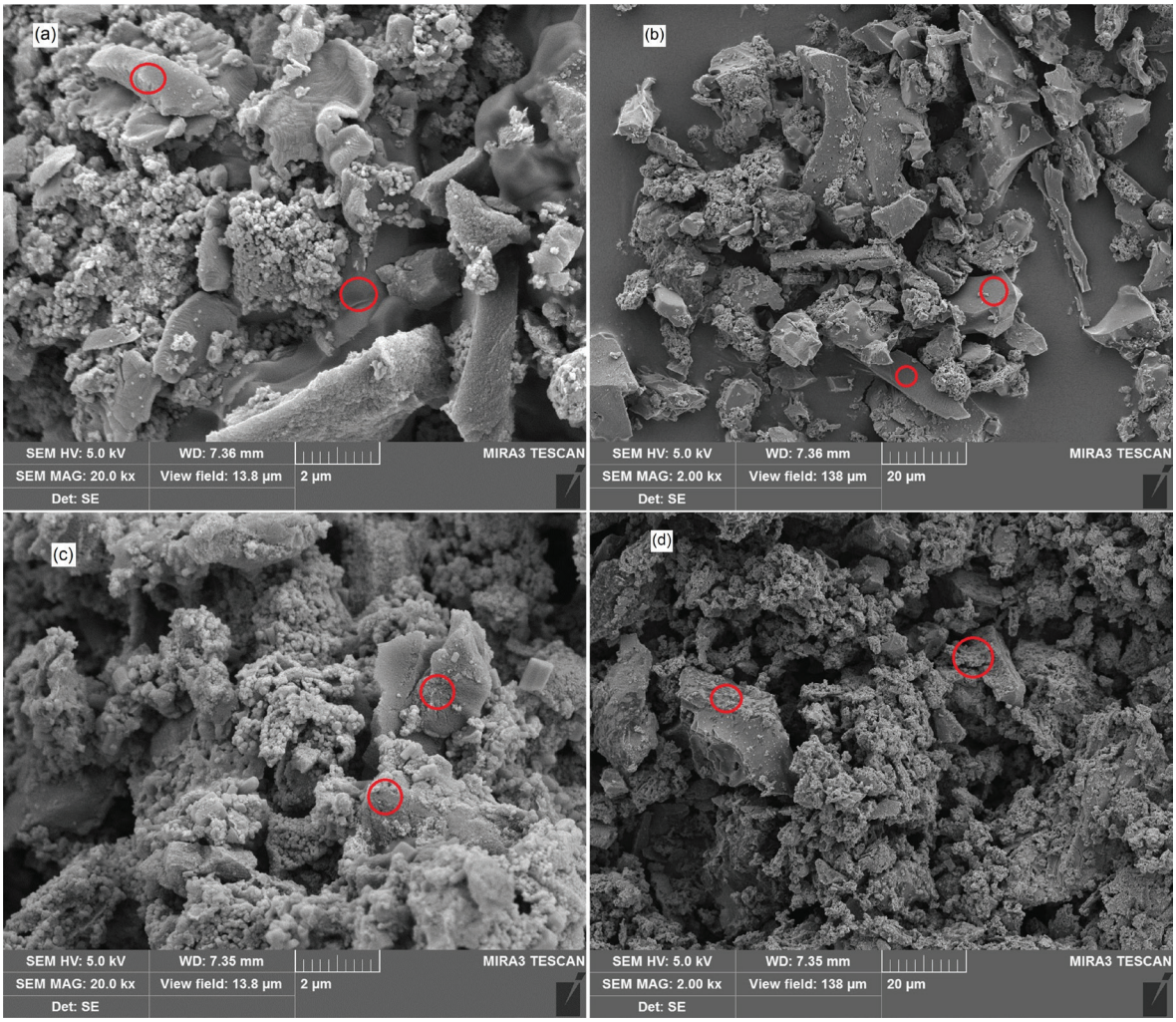

Figure 3. SEM images of deoxidizers before and after reaction. (a) Mn/AC_2 before reaction; (b) Mn/AC_2 after reaction; (c) Mn/AC_1 before reaction; (d) Mn/AC_1 after reaction.

TG analysis

Figure 4 shows the TG and DTG (derivative thermogravimetry) curves for the Mn/AC_1, Mn/AC_2 and Mn/AC_3 deoxidizer. For Mn/AC_2, it can be seen that the weight loss of the deoxidizer in the temperature range of 40-800 °C can be divided into two segments. The weight loss below 200 °C is mainly due to the evaporation of free water and internal water in the deoxidizer. The weight loss step after the temperature is between 200 and 500 °C is mainly caused by the oxidation reaction of the deoxidizer with oxygen in the air.[17] In addition, it can be seen from the DTG curve that after the temperature is higher than 200 °C, the DTG rapidly decreases, and then tends to be stable after 500 °C. It shows that the deoxidation efficiency of the deoxidizer is higher at 200-500 °C. The weight loss of the deoxidizer is about 59 wt.% between 200-500 °C. Compared with Mn/AC_2, Mn/AC_3 have three weight loss stages: the first stage, which occurs at temperatures between 100 to 200 °C, another stage at 300-500 °C with weight loss of ca. 35 wt.%, and the third stage occurred at temperatures higher than 700 °C. It demonstrated that the content of carbon, which is easy to be oxidized into CO_2 on Mn/AC_3 is higher than Mn/AC_2. The shape of DTG curve of Mn/AC_1 is similar to Mn/AC_3, the second weight loss stage occurs at temperature between 200-600 °C with weight loss of ca. 60 wt.%.

FTIR analysis

Figure 5 displays FTIR of six deoxidizers before and after reaction. As shown in Figures 5a and 5b, for AC_x deoxidizer, absorption peaks at approximately 3420, 1598, and 1087 cm^{-1} was observed. The absorption peak at 3420 cm^{-1} belongs to the stretching vibrations of hydroxyl, carboxyl, and surface adsorbed water.[29,31-34] The absorption peak at 1560-1510 cm^{-1} with the main adsorption at 1598 cm^{-1} contributed to the C=O stretching vibration of different functional groups, including ketone and carbonyl.[31-33] The peak at 1300-900 cm^{-1} with the main adsorption at 1087 cm^{-1} belonged to the presence of the C–O stretching of ester and C–OH.[31,35-38] After the reaction (Figure 5b), it has been found that the absorption peak of AC_1 and AC_2 deoxidizer at 1087 cm^{-1} had no significant change. However, the AC_3 absorption peak was significantly reduced at 1087 cm^{-1}, while the peak at 1598 cm^{-1} was significantly enhanced and a new peak was produced at 1750 cm^{-1}. The difference of the intensity and the slight shift of wavenumber of samples suggested a small difference in the surface chemistry of the samples.[31,39] This indicates that AC_3 deoxidizer has good deoxidation activity. This is also consistent with the experimental results of deoxidation.

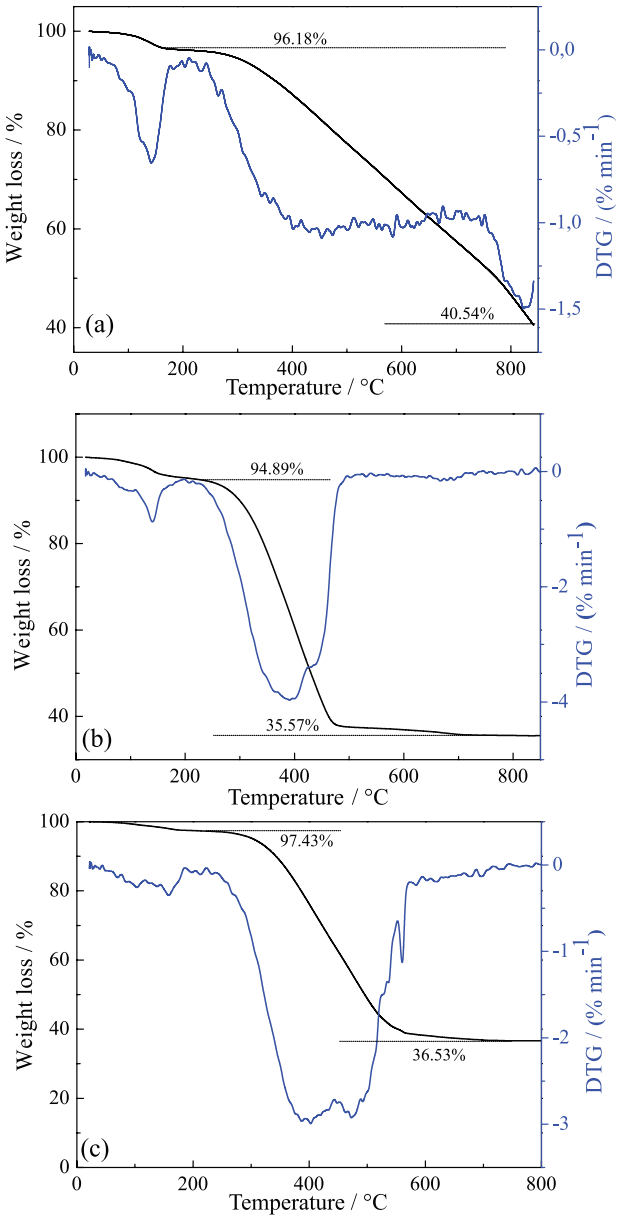

Figure 4. TG/DTG curves of (a) Mn/AC_2; (b) Mn/AC_3; (c) Mn/AC_1 under air.

FTIR of AC_x modification with potassium permanganate before and after reaction is shown in Figures 5c and 5d. As can be seen from the figure, for Mn/AC_x deoxidizer, absorption peaks at approximately 3420, 1655, 1450, 1087 and 601 cm^{-1} was detected. The absorption peak at 3420 cm^{-1} belonged to hydroxyl OH absorption peak; the one at approximately 1655 cm^{-1} belonged to the stretching (C=O) vibrations of carboxyl and carbonyl in acidic oxygen surface groups, which in turn play a vital role in metal adsorption.[29,37] The peak at 1450 cm^{-1} belonged to C–H stretching vibrations of methyl.[38,40] The peak at 601 cm^{-1}

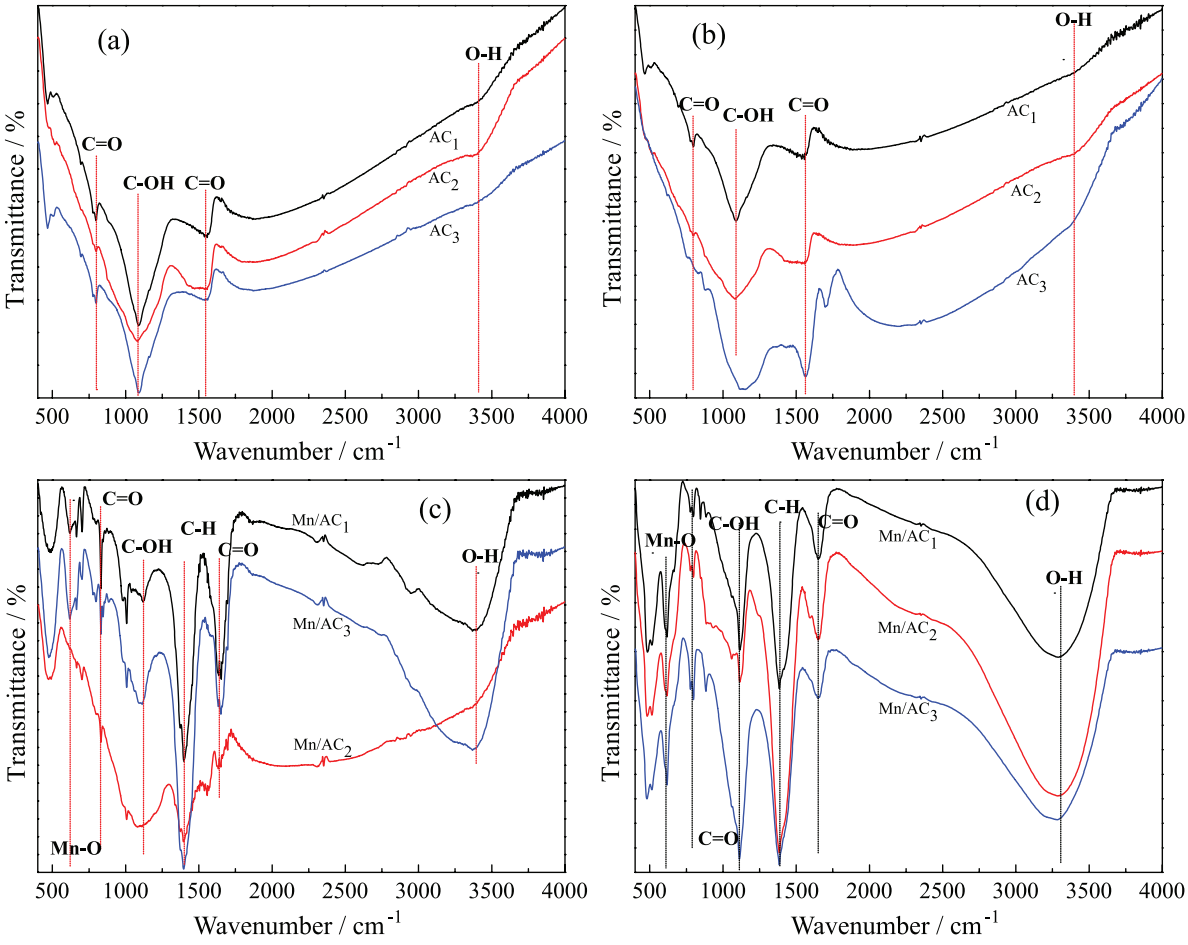

Figure 5. FTIR of six deoxidizers: (a) AC_x (x = 1, 2, 3) before reaction; (b) AC_x (x = 1, 2, 3) after reaction; (c) Mn/AC_x (x = 1, 2, 3) before reaction; (d) Mn/AC_x (x = 1, 2, 3) after reaction.

belonged to the characteristic absorption of Mn−O.[41] Compared with unmodified deoxidizer, it was found that two new peaks were produced at 1450 and 601 cm^{-1} for Mn/AC_x deoxidizer. Except for the two newly generated peaks, the peak positions of AC_2 and Mn/AC_2 did not substantially change. The peak strengths of Mn/AC_1 and Mn/AC_3 at 3420, 1655 and 1087 cm^{-1} were significantly stronger than those of AC_1 and AC_3. C−OH absorption peak at 1087 cm^{-1} decreased, which is due to that under acid condition, the strong oxidizing potassium permanganate reacts with C−OH in activated carbon.[38,42] After reaction, the absorption peak at 1087 cm^{-1} was improved for all modified deoxidizer. Moreover, the absorption peaks at 3420, 1655 and 1450 cm^{-1} were obviously improved for Mn/AC_2 deoxidizer. These changes indicate that electron transfer occurred between functional groups and Mn during the reaction. However, after the reaction, the other absorption peaks did not change significantly on Mn/AC_1 and Mn/AC_3, which indicates that the deoxidation activity of Mn/AC_1 and Mn/AC_3 is lower than that of Mn/AC_2.

XPS analysis

XPS studies were performed to determine the surface chemical state and elemental composition of Mn/AC_2 deoxidizer before and after reaction. The XPS survey spectrum of the representative sample Mn/AC_2 verifies the elements presence of Mn, C and O, as shown as follows.

XPS analysis of manganese element

The XPS patterns of the Mn 2p region for Mn/AC_2 deoxidizer are presented in Figures 6a and 6b. It can be found that the binding energy peak of Mn $2p_{3/2}$ and Mn $2p_{1/2}$ was located at about 642.1 and 653.8 eV, respectively, with an energy separation of 11.3 eV. The Mn $2p_{3/2}$ spectra were fitted with two characteristic peaks, which were assigned to Mn^{3+} and Mn^{4+} at 641.7 and 644.7 eV, respectively. Mn^{4+} and Mn^{3+} are considered to be the main valence states affecting the deoxidation properties of the deoxidizer.[20,31,43-49] In order to accurately determine the oxidation state of manganese, Mn 3s analysis was performed, as shown in Figures 6c and 6d. It can be found that the Mn 3s core level peak of

Mn/AC_2 deoxidizer shows peak splitting, and peak energy separation (ΔE) is observed at 5.15 eV.[50,51] According to the linear relationship between ΔE and the oxidation state of manganese, the average oxidation state of Mn is 3.5 for the Mn/AC_2 deoxidizer. After the deoxidation reaction, no valence change of Mn was observed from Figure 6b. However, it can be clearly seen from the analysis of Mn 3s (Figure 6d) that the peak energy separation (ΔE) is significantly smaller, from the original 5.15 to 4.92. Based on the linear relationship between ΔE and the oxidation state of manganese, the Mn average oxidation state of the Mn/AC_2 deoxidizer increased from 3.5 to 3.6/3.7.

XPS analysis of carbon element

Figure 7 shows the C 1s spectra of Mn/AC_2 deoxidizer before and after reaction. The C 1s spectra could be divided into three peaks at 284.5, 285.0, and 286.8 eV, which indicates that there are different types of carbon species on deoxidizer surface.[52] According to XPS standard values and related data, the binding energy at 284.5 eV was assigned to graphite-like C–C carbon, the binding energy at 285.0 assigned to alkyl C–C carbon, and the binding energy at 286.4-286.9 eV to carbonyl C=O carbon. By comparing the results of Figures 7a and 7b, it can be found that the intensity of the graphite-like C–C carbon structure increases, the alkyl C–C carbon disappears, and the peak width of the carbonyl C=O carbon decreases. This indicates that the alkyl C–C carbon which is easily oxidized completely reacts with oxygen during the reaction. Due to the low reactivity of graphite carbon, the relative content in the sample is higher after the deoxidation reaction.

XPS analysis of oxygen element

Figure 8 shows XPS patterns of the O 1s for Mn/AC_2 deoxidizer before and after reaction. For the O 1s spectra of Mn/AC_2 deoxidizer, it can be found that two peaks were observed. It indicates that the different types of oxygen species are present on the surface of the deoxidizer. The peaks at 529-531 eV is attributed to the binding energy of the lattice oxygen of the Si–O bond in the AC framework and the Mn–O–Mn bond of the Mn/AC_2 deoxidizer. The binding energy of 531-534 eV is attributed to chemisorbed oxygen. They can be assigned to defect oxides or the surface

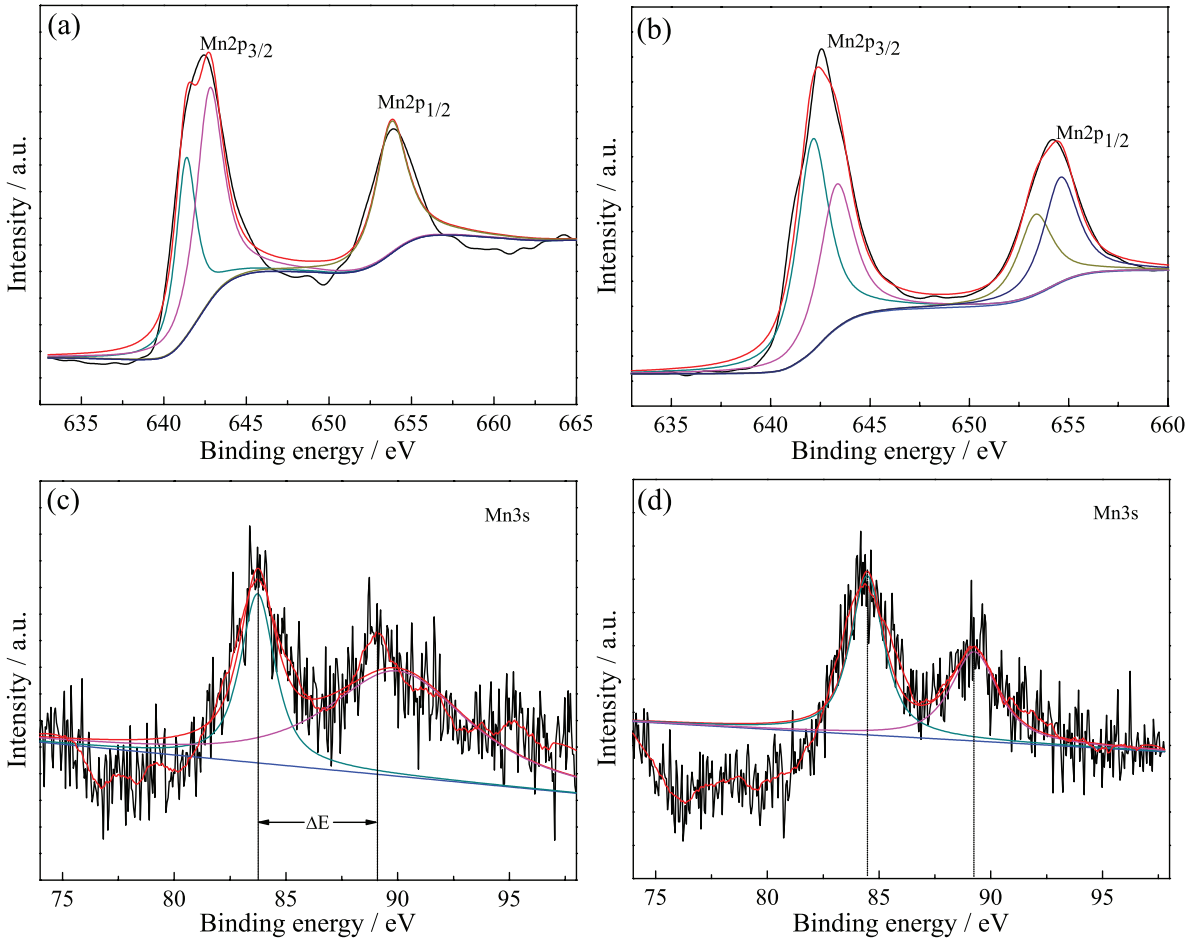

Figure 6. Mn spectra of Mn/AC_2 deoxidizer. (a) Mn 2p before reaction; (b) Mn 2p after reaction; (c) Mn 3s before reaction; (d) Mn 3s after reaction.

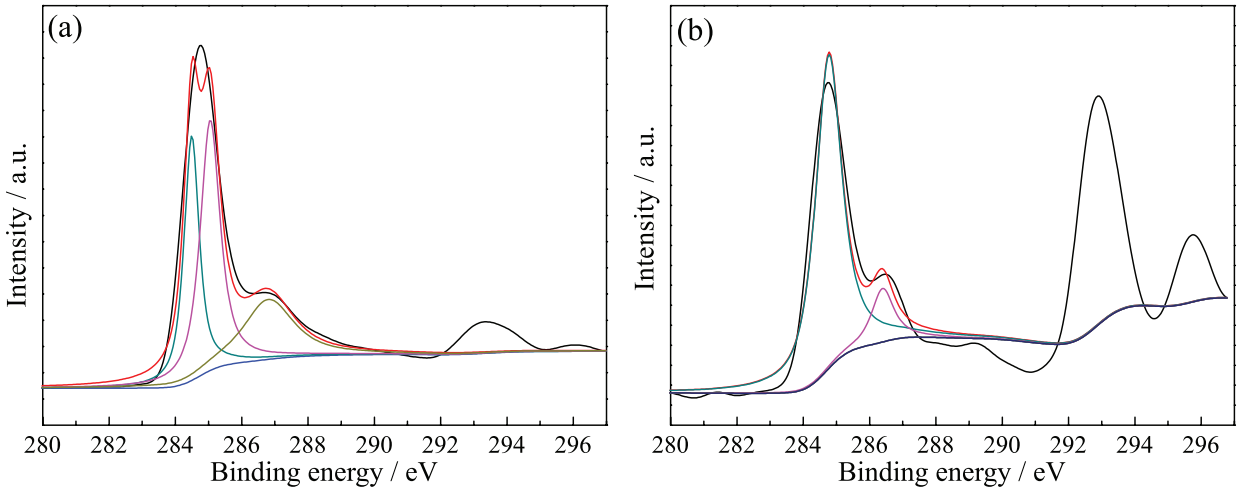

Figure 7. C 1s spectra of Mn/AC_2 deoxidizer (a) before and (b) after reaction.

oxygen ions with a low coordination. The abundance of chemisorbed oxygen, which has a higher mobility than the lattice oxygen in the Mn/AC_2 deoxidizer, was important for the low concentration coalbed methane deoxidation reaction. Comparing Figures 8a and 8b, the ratio of chemisorbed oxygen to lattice oxygen is significantly reduced after the reaction, this also demonstrates that the deoxidation activity of Mn/AC_2 deoxidizer decreased with reaction time.

Deoxidation performance

Higher deoxidation temperature is beneficial to oxidative deoxidation reaction, however, too high deoxidation temperature will cause decomposition or oxidation of methane, which is not conducive to methane enrichment. Therefore, temperature is a critical operating variable for deoxidation.[17,53] Figure 9 shows the deoxidation activity of different deoxidizers at different deoxidation temperatures.

It can be seen that the original three activated carbons AC_x (x = 1,2,3) exhibit the same deoxidation activity at different deoxidation temperatures. The order of activity is $AC_3 > AC_2 > AC_1$. With the increase of deoxidation temperature, the deoxidation activity of activated carbon AC_2 and AC_1 remained unchanged. However, the deoxidation activity of activated carbon AC_3 gradually increased. For AC_3, the total deoxidation time (oxygen content < 0.5%) can be maintained for about 100 min at a deoxidation temperature of 300 °C, and the complete deoxidation time can be maintained for about 300 min when the deoxidation temperature is increased to 300 °C. This difference is mainly due to that the activated carbon is made of different materials. Although activated carbons AC_1 and AC_2 are both coal-based activated carbon, the activity of AC_2 is slightly higher than that of AC_1, which could be attributed to the pore characteristic parameters (specific surface area, pore volume and pore diameter) of AC_2 being superior to AC_1. However, compared with the specific surface area of the three activated carbons, the specific surface area of AC_3 is

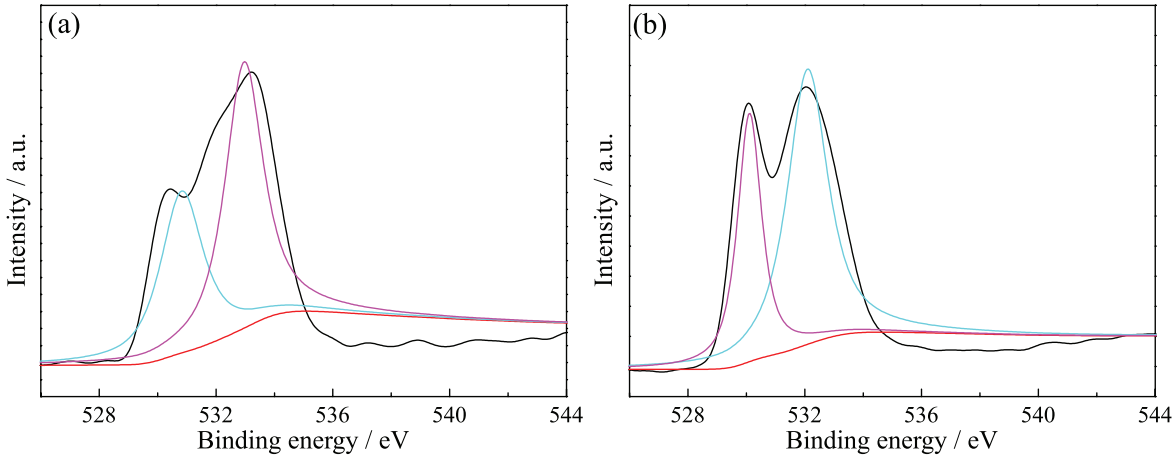

Figure 8. O 1s spectra of Mn/AC_2 deoxidizer (a) before and (b) after reaction.

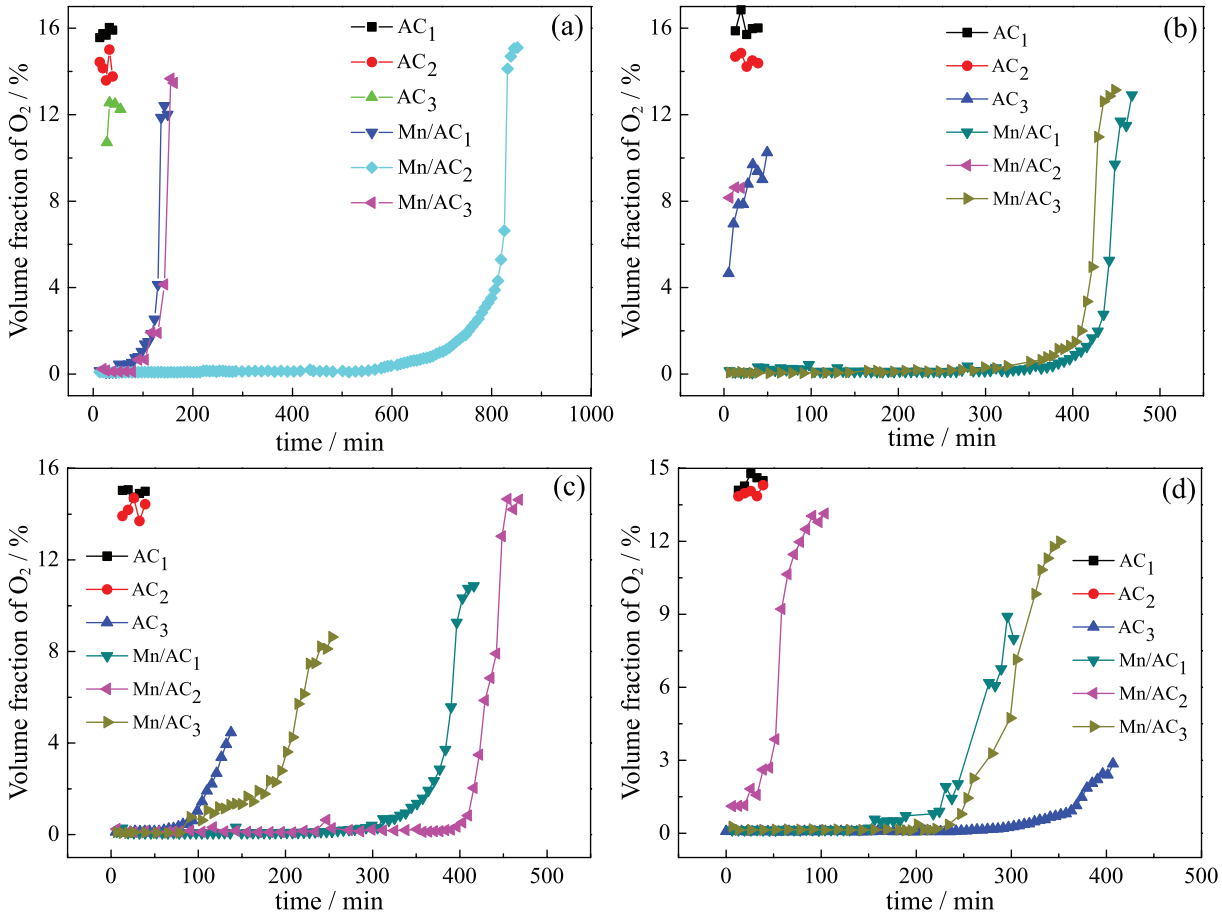

Figure 9. Reactive activity of the different deoxidizers at the different temperature showing oxygen concentration of outlet gas at (a) 200; (b) 250; (c) 300 and (d) 350 °C.

significantly lower than that of AC_1 and AC_2, which indicates that the deoxidizing activity of different kinds of deoxidizers is not only related to the physical structure of oxidants, but also correlated with material itself being made.

The deoxidation activity of Mn/AC_x (x = 1, 2, 3) deoxidizer obtained was significantly improved compared with unmodified. Under the deoxidation condition of 200 °C, Mn/AC_2 showed the best oxidation performance among all the potassium permanganate modified deoxidizer, and the time of complete deoxidation could reach about 600 min. After further increasing the deoxidation temperature to 250 °C, the deoxidation activity of Mn/AC_1 and Mn/AC_3 is also greatly improved, and the time for complete deoxidation of both can reach about 400 min. The deoxidation rate of Mn/AC_2 is relatively low, about 50%. This is mainly due to the fact that at the deoxidation at 200 °C, more active functional groups and carbon materials are substantially consumed; while the relatively stable carbon species require higher activation energy to react with oxygen. As can be seen from Figure 9c, as the deoxidation temperature is further increased, the deoxidation activity of Mn/AC_x (x = 1, 2, 3) is further excited. However, when the deoxidation temperature increases to 350 °C, the deoxidation rate of Mn/AC_2 rapidly decreases. This is mainly due to the fact that after deoxidation at 200-300 °C for nearly 1250 min, the carbon material with higher activity in Mn/AC_2 is basically consumed. In addition, comparing Figures 9a-9d, it can be clearly found that the modified deoxidizer Mn/AC_x (x = 1, 2, 3) can significantly reduce the activation energy of the deoxidation reaction and improve the deoxidation characteristics of the sample. This is mainly because on the one hand potassium permanganate is a strong oxidizing substance and doping Mn as an additive in AC can react to its physicochemical properties and improves the reactive activity. On the other hand, after modification with potassium permanganate, the added Mn has a certain activity, which can promote the deoxidation reaction and reduce the activation energy of the deoxidation reaction. As can be seen from the comparison of Figures 9b and 9d, for AC_3 and Mn/AC_3 deoxidizers, the complete deoxidation starting temperatures were 250 and 350 °C, respectively; and the total deoxidation retention time was approximately 300 and 350 min, respectively. This indicates that the deoxidation temperature is reduced by at least

100 °C after modification with potassium permanganate. This provides a strong guarantee for deoxidation and enrichment of oxygen-containing coalbed methane, reducing methane loss and deoxidation temperature.

Conclusions

In a fixed-bed reactor, low-concentration coalbed methane deoxidation has been studied over different deoxidizers. The results show that the addition of potassium permanganate on AC_x has greatly improved the deoxidation ability, compared with the original activated carbon AC_x. Mn/AC_2 catalyst exhibited the best deoxidation activity at 200-350 °C among all the AC_x and Mn/AC_x deoxidizers. It indicates the modified deoxidizers lead to significant reduction of reaction barriers in the deoxidation reaction, which means that activated carbon is more favorable for oxygen adsorption and dissociation after potassium permanganate modification. In addition, due to the good adsorption performance of activated carbon, a large amount of manganese species is adsorbed on the surface of the activated carbon during the modification process. When activated carbon is used both as a carrier and as a reactant, these manganese species act as catalytically active components to promote the oxidation reaction. Under the combined action of the above several aspects, the activation energy of the oxidation reaction is lowered, and the deoxidation activity of Mn/AC_x is improved. Also, the functional groups on the surface of the activated carbons and valence state of metal and oxidized form have a certain type of influence on the activity of the deoxidating reaction.

Supplementary Information

Supplementary data (adsorption-desorption curves, pore size distribution and EDS mapping pattern) are available free of charge at http://jbcs.sbq.org.br as a PDF file.

Acknowledgments

This work was supported by the National Natural Science Foundation of China (Nos. U1610115, 21676174 and 21878200), International S&T Cooperation Program of Shanxi Province (201703D421038), Shanxi Scholarship Council of China (2017-036), and Joint Fund of Shanxi Provincial Coal Seam Gas (2015012019).

References

1. Yang, Z.; Liu, J.; Zhang, L.; Zheng, S.; Guo, M.; Yan, Y.; *RSC Adv.* **2014**, *4*, 39394.
2. Cheng, Y. P.; Wang, L.; Zhang, X. L.; *Int. J. Greenhouse Gas Control* **2011**, *5*, 157.
3. Zhang, Q. F.; Wu, X. P.; Zhao, G. F.; Li, Y. K.; Wang, C. Z.; Liu, Y.; Gong, X. Q.; Lu, Y.; *Chem. Commun.* **2015**, *51*, 12613.
4. Karacan, C. Ö.; Ruiz, F. A.; Cotè, M.; Phipps, S.; *Int. J. Coal Geol.* **2011**, *86*, 121.
5. Li, Q. Y.; Wang, L.; Ju, Y. L.; *CIESC J.* **2011**, *62*, 1471.
6. Cui, G.; Li, Z. L.; Zhao, Y. L.; *RSC Adv.* **2015**, *5*, 68218.
7. Li, Y. L.; Liu, Y. S.; Yang, X.; *Sep. Sci. Technol.* **2013**, *48*, 1201.
8. Li, Y. L.; Liu, Y. S.; *Int. J. Coal Prep. Util.* **2013**, *33*, 72.
9. Li, Y. L.; Liu, Y. S.; Yang, X.; *Adv. Mater. Res.* **2011**, *233-235*, 2276.
10. Zhen, L.; Grande, C. A.; Ping, L.; Yu, J.; Rodrigues, A. E.; *Sep. Purif. Technol.* **2011**, *81*, 307.
11. Zhou, Y.; Fu, Q.; Shen, Y.; Sun, W.; Zhang, D.; Li, D.; Yan, H.; *Energy Fuels* **2016**, *30*, 1496.
12. Yang, X.; Liu, Y. S.; Li, Y. L.; Zhang, C. Z.; Meng, Y.; Yang, H. J.; *J. China Coal Soc.* **2011**, *36*, 91.
13. Lopes, F. V. S.; Grande, C. A.; Rodrigues, A. E.; *Chem. Eng. Sci.* **2011**, *66*, 303.
14. Gomes, G. V.; Hassan, M. M.; *Sep. Purif. Technol.* **2001**, *24*, 189.
15. Shimada, S.; Yoshitake, J.; *J. Jpn. Inst. Energy* **2013**, *92*, 536.
16. Zhao, P.; Zhang, G.; Sun, Y.; Xu, Y.; *Environ. Sci. Pollut. Res.* **2017**, *24*, 15240.
17. Hu, P.; Pan, H.; Lin, Q.; Cao, J.; Zhang, Y.; Zhao, M.; *Energy Fuels* **2018**, *32*, 6136.
18. Yang, L.; Huang, T.; Jiang, X.; Jiang, W.; *Adsorption* **2016**, *22*, 1099.
19. Lee, Y. W.; Park, J. W.; Choung, J. H.; Choi, D. K.; *Environ. Sci. Technol.* **2002**, *36*, 1086.
20. Wu, J.; Zhao, Z.; Huang, T.; Sheng, P.; Zhang, J.; Tian, H.; Zhao, X.; Zhao, L.; He, P.; Ren, J.; Gao, K.; *Catal. Commun.* **2017**, *93*, 62.
21. Li, W.; Tan, S.; Shi, Y.; Li, S.; *Fuel* **2015**, *160*, 35.
22. Biniak, S.; Szymański, G.; Siedlewski, J.; Światkowski, A.; *Carbon* **1997**, *35*, 1799.
23. Arena, F.; Torre, T.; Raimondo, C.; Parmaliana, A.; *Phys. Chem. Chem. Phys.* **2001**, *3*, 1911.
24. Gil, A.; Gandía, L. M.; Korili, S. A.; *Appl. Catal., A* **2004**, *274*, 229.
25. Mirzaei, A. A.; Shaterian, H. R.; Kaykhaii, M.; *Appl. Surf. Sci.* **2005**, *239*, 246.
26. Huang, Z. B.; Liu, B. S.; Wang, X. H.; Tang, X. Y.; Amin, R.; *Ind. Eng. Chem. Res.* **2015**, *54*, 11268.
27. Shukla, P. R.; Wang, S.; Sun, H.; Ang, H. M.; Tadé, M.; *Appl. Catal., B* **2010**, *100*, 529.
28. Chella, S.; Kollu, P.; Komarala, E. V. P.; Doshi, S.; Saranya, M.; Felix, S.; Ramachandran, R.; Saravanan, P.; Koneru, V. L.; Venugopal, V.; Jeong, S. K.; Gracea, A. N.; *Appl. Surf. Sci.* **2015**, *327*, 27.

29. Zhang, J. J.; Wang, W. Y.; Shen, L. P.; Wang, G. J.; Song, H.; *Adsorpt. Sci. Technol.* **2016**, *34*, 331.
30. Pang, M.; Long, G.; Jiang, S.; Ji, Y.; Han, W.; Wang, B.; Liu, X.; Xi, Y.; *Electrochim. Acta* **2015**, *161*, 297.
31. Tian, Z.; Wang, C.; Si, Z.; Ma, L.; Chen, L.; Liu, Q.; *Appl. Catal., A* **2017**, 5*41*, 50.
32. Yang, H.; Yan, R.; Chen, H.; Lee, D. H.; Liang, D. T.; Zheng, C.; *Energy Fuels* **2006**, *20*, 1321.
33. Yang, H.; Yan, R.; Chen, H.; Lee, D. H.; Zheng, C.; *Fuel* **2007**, *86*, 1781.
34. Zhang, L.; Chang, X.; Li, Z.; He, Q.; *J. Mol. Struct.* **2010**, *964*, 58.
35. Gomez-Serrano, V.; Pastor-Villegas, J.; Perez-Florindo, A.; Duran-Valle, C.; Valenzuela-Calahorro, C.; *J. Anal. Appl. Pyrolysis* **1996**, *36*, 71.
36. Sun, F.; Gao, J.; Zhu, Y.; Qin, Y.; *Korean J. Chem. Eng.* **2011**, *28*, 2218.
37. Li, Z.; Li, J.; Wang, Y.; Wei, Y.; *Spectrochim. Acta, Part A* **2014**, *117*, 422.
38. Yang, L.; Jiang, X.; Yang, Z. S.; Jiang, W. J.; *Ind. Eng. Chem. Res.* **2015**, *54*, 1689.
39. Fan, L.; Chen, J.; Guo, J.; Jiang, X.; Jiang, W.; *J. Anal. Appl. Pyrolysis* **2013**, *104*, 353.
40. Erabee, I. K.; Ahsan, A.; Jose, B.; Aziz, M. M. A.; Ng, A. W. M.; Idrus, S.; Daud, N. N. N.; *KSCE J. Civ. Eng.* **2018**, *22*, 1083.
41. Wang, M.; Zhang, P.; Li, J.; Jiang, C.; *Chin. J. Catal.* **2014**, *35*, 335.
42. Zhang, G.; Sun, Y.; Zhao, P.; Xu, Y.; Su, A.; Qu, J.; *J. CO2 Util.* **2017**, *20*, 129.
43. Fan, L.; Jiang, X.; Jiang, W.; Guo, J.; Chen, J.; *Adsorption* **2014**, *20*, 747.
44. Biesinger, M. C.; Lau, L. W.; Gerson, A. R.; Smart, R. S. C.; *Appl. Surf. Sci.* **2010**, *257*, 887.
45. Chen, J.; Zhu, B.; Sun, Y.; Yin, S.; Zhu, Z.; Li, J.; *J. Braz. Chem. Soc.* **2018**, *29*, 79.
46. Dai, F.; Yu, Y.; Meng, M.; Zhang, J.; Zheng, L.; Hu, T.; *Catal. Lett.* **2014**, *144*, 1210.
47. Jang, D. I.; Park, S. J.; *Fuel* **2012**, *102*, 439.
48. Deng, J.; He, S.; Xie, S.; Yang, H.; Liu, Y.; Guo, G.; Dai, H.; *Environ. Sci. Technol.* **2015**, *49*, 11089.
49. Gallegos, M. V.; Peluso, M. A.; Finocchio, E.; Thomas, H. J.; Busca, G.; Sambeth, J. E.; *Chem. Eng. J.* **2017**, *313*, 1099.
50. Galakhov, V. R.; Demeter, M.; Bartkowski, S.; Neumann, M.; Ovechkina, N. A.; Kurmaev, E. Z.; Lobachevskaya, N. I.; Mukovskii, Y. M.; Mitchell, J.; Ederer, D. L.; *Phys. Rev. B: Condens. Matter Mater. Phys.* **2002**, *65*, 113102.
51. Li, L.; Diao, Y.; Xiu, X.; *J. Rare Earth* **2014**, *32*, 409.
52. Seok, S. H.; Han, S. H.; Lee, J. S.; *Appl. Catal., A* **2001**, *215*, 31.
53. Ren, J.; Xie, C.; Lin, J.; Li, Z.; *Process Saf. Environ. Prot.* **2014**, *92*, 896.

Submitted: November 14, 2018
Published online: May 8, 2019